Published online 27 June 2017

Nucleic Acids Research, 2017, Vol. 45, No. 16 ***9625–9639***
doi: 10.1093/nar/gkx570

The important conformational plasticity of DsrA sRNA for adapting multiple target regulation

Pengzhi Wu, Xiaodan Liu, Lingna Yang, Yitong Sun, Qingguo Gong, Jihui Wu* and Yunyu Shi*

Hefei National Laboratory for Physical Sciences at Microscale and School of Life Sciences, University of Science and Technology of China, Anhui 230027, China

Received December 15, 2016; Revised June 01, 2017; Editorial Decision June 15, 2017; Accepted June 22, 2017

ABSTRACT

In bacteria, small non-coding RNAs (sRNAs) could function in gene regulations under variable stress responses. DsrA is an ∼90-nucleotide Hfq-dependent sRNA found in *Escherichia coli*. It regulates the translation and degradation of multiple mRNAs, such as *rpoS*, *hns*, *mreB* and *rbsD* mRNAs. However, its functional structure and particularly how it regulates multiple mRNAs remain obscure. Using NMR, we investigated the solution structures of the full-length and isolated stem–loops of DsrA. We first solved the NMR structure of the first stem–loop (SL1), and further studied the melting process of the SL1 induced by the base-pairing with the *rpoS* mRNA and the A-form duplex formation of the DsrA/*rpoS* complex. The secondary structure of the second stem–loop (SL2) was also determined, which contains a lower stem and an upper stem with distinctive stability. Interestingly, two conformational states of SL2 in dynamic equilibrium were observed in our NMR spectra, suggesting that the conformational selection may occur during the base-pairing between DsrA and mRNAs. In summary, our study suggests that the conformational plasticity of DsrA may represent a special mechanism sRNA employed to deal with its multiple regulatory targets of mRNA.

INTRODUCTION

Small non-coding RNAs (sRNAs) are widespread among all kingdoms, and play the critical regulatory roles in many cellular processes (1,2). In bacteria, sRNAs are typically 50–300 nucleotides in length, and are highly expressed during adaptation to changes in the environment, including low ion concentration, oxidative stress, outer membrane stress or nutrient starvation (3,4). The major class of bacterial regulatory sRNAs acts by imperfectly base pairing with their target mRNAs in *trans*, usually affecting the translation and stability of mRNAs (5,6). These sRNAs usually bind to the 5′ untranslated region (UTR) of the mRNAs, often occluding the ribosome-binding site (RBS) and/or starting codons (7). The formation of this sRNA/mRNA duplex usually leads to translational inhibition and/or mRNA degradation (8,9). However, sRNA can also activate the expression of its target mRNA by competing with the formation of a stem–loop structure, which normally sequesters the RBS and inhibits its translation (10,11). The RNA chaperone Hfq is crucial for this *trans*-encoded sRNA regulation by facilitating the direct interaction between sRNAs and their target mRNAs (12,13).

DsrA (downstream of rcsA), an ∼90-nucleotide Hfq-dependent RNA from *Escherichia coli*, is one of the first regulator sRNAs that have been identified to regulate multiple mRNAs (14,15). It is encoded by a gene in the downstream region of *rcsA*, which is a positive regulator of capsular polysaccharide synthesis (16). Upon low temperature or acidic pH stress, DsrA is highly expressed to modulate the translations of *rpoS* and *hns* mRNAs that encode two global transcription regulators, the alternative sigma factor σ^S and the nucleoid-structuring protein H-NS (14,15,17,18). DsrA was also shown recently to negatively regulate *mreB* and *rbsD* mRNAs, which are involved in the cell wall biosynthesis and the ribose metabolism, respectively (19,20).

It has been previously indicated that DsrA contained three stem–loop structures, denoted SL1, SL2 and SL3, and a long linker between SL1 and SL2 (Linker1) (Figure 1) (21). The SL1 and its 3′ following sequence in DsrA sRNA positively regulate the expression of *rpoS* mRNA by an anti-antisense mechanism (15,22). *rpoS* mRNA usually forms a large stem–loop structure upstream from the start codon that inhibits the ribosome binding (23). When DsrA binds to the upstream region in the 5′-UTR of *rpoS*, it disrupts this stem–loop to release the RBS and activates the translation of *rpoS* mRNA efficiently (23). The DsrA activation of *rpoS* translation is Hfq-dependent (24). Hfq forms a stable ternary complex with DsrA and *rpoS* mRNA, increas-

*To whom correspondence should be addressed. Tel: +86 551 63607464; Fax: +86 551 63601443; Email: yyshi@ustc.edu.cn
Correspondence may also be addressed to Jihui Wu. Tel: +86 551 63603745; Fax: +86 551 63601443; Email: wujihui@ustc.edu.cn

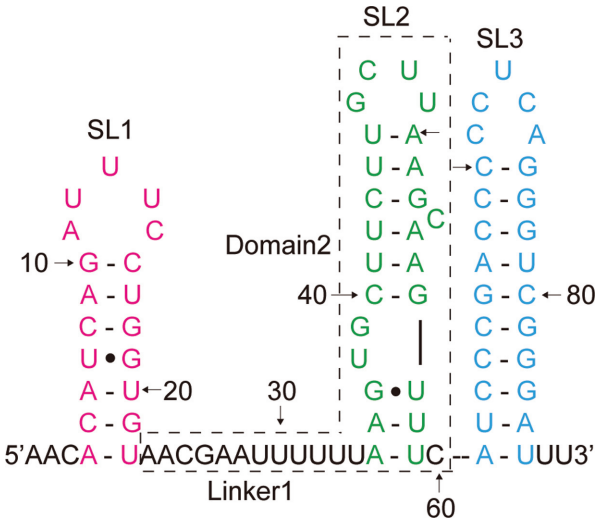

Figure 1. Schematic of the secondary structure of DsrA. Three stem–loops are colored magenta, green and cyan. The DsrA-Domain2 consists of nucleotides in the dashed box. The single strand linker between SL1 and SL2 is labeled as Linker1. Watson–Crick hydrogen bonds are indicated by continuous lines and G•U wobble base pairs are denoted by a circle.

ing the annealing rate of DsrA to *rpoS* (25). However, the DsrA/*rpoS* duplex formation *in vivo* does not need Hfq but may requires CsdA helicase (26). Moreover, base-pairing of DsrA with *rpoS* mRNA protects *rpoS* from the degradation by RNase E (27). Recently, it has been reported that the annealing of DsrA within the *rpoS* 5′-UTR region also represses the premature termination of the Rho-dependent transcription (28).

A portion of the Linker1 and the SL2 of DsrA participates to the base-pairing with *hns*, *mreB* or *rbsD* mRNAs, blocking mRNAs translation and/or degradation (19,20,29). NMR and SAXS experiments have revealed that the SL2 is very dynamic, unfolding into an extended and single-stranded conformation when binding to Hfq (30). SL3, which contains many G–C base pairs with a short poly-U tract, is a Rho-independent transcriptional terminator (22). Three alternative DsrA secondary structures have also been proposed by using the program MULFOLD, nuclease footprinting analysis, and the isoenergetic microarray mapping method (14,29,31,32). The four secondary structural predictions of DsrA all contain three stem–loops which are identical in SL1 and SL3 but not for Linker1 and SL2. The full-length DsrA is able to self-assemble into a large polymer *in vitro*, resulting from the auto-assembly of the 22-nucleotide central region of DsrA (33–35).

Despite the importance of DsrA sRNA in post-transcriptional regulation, its atomic-level resolution structure has not been published. In addition, sRNA has been shown to directly regulate multiple mRNAs that could balance the different transcriptional responses at the post-transcriptional level (36). However, the mechanism of sRNA-mediated regulation of multiple, structurally unrelated mRNAs is less understood at the molecular level. Previous work has shown that a conserved G/U-rich region within GcvB sRNA was required for its base-pairing with multiple targets (37). In this work, we propose that multiple targets can also be relevant to the different conformational states for a given sRNA.

In this research, we determined the 3D structure of DsrA-SL1 by NMR, which forms a stable stem–loop structure adopting a typical A-form helix with a dynamic AUUUC pentaloop. Native PAGE and NMR experiments confirm that the 5′ UTR of *rpoS* mRNA base pairs with DsrA and unwinds DsrA-SL1, and the DsrA/*rpoS* complex forms an A-form duplex structure. We also investigated the secondary structure of Domain2 RNA, which contains the unpaired Linker1 and SL2 of DsrA. The NMR data reveals two conformational states of SL2 in solution which may be in dynamic equilibrium. Based on these results, we proposed a model for multiple mRNA sequestration by DsrA.

MATERIALS AND METHODS

RNA sample preparation and purification

The DNA sequence of the full-length DsrA sRNA was designed to include the T7 RNA polymerase promoter, the RNA coding sequence, and restriction sites for EcoRI and XbaI. The target was generated by one polymerase chain reaction (PCR) with four overlapping primers (FL_1f, FL_2r, FL_3f and FL_4r). After ligating into the pUC19 plasmid, the plasmid was sequenced (Invitrogen) to confirm the identity of the insert and/or mutations. RNA samples were synthesized by *in vitro* transcription with T7 RNA polymerase in 10 mL reactions. The template for full-length DsrA was a PCR product at 0.3 μM amplified from the target plasmid using primers FL_5tem and FL_3tem. The templates of the other RNAs were 0.3 μM synthetic template oligonucleotide DNA and 0.3 μM synthetic promoter oligonucleotide DNA (5′-GAAATTAATACGACTCACTATAG -3′). All oligonucleotide DNA primers and templates can be seen in Supplementary Table S1. The *in vitro* transcription mixture contained 40 mM Tris–HCl (pH 8.1), 1 mM spermidine, 0.01% (v/v) Triton X-100, 10 mM DTT, 20–50 mM $MgCl_2$, 1 mg T7 RNA polymerase and 5 mM each of unlabeled or uniformly ^{13}C,^{15}N-labeled NTPs (SILANTES GmbH). Optimal concentration of $MgCl_2$ was determined in small-scale reactions.

The reactions were incubated for 4 h in a water bath at 37°C, and then quenched by the addition of 0.1 volume of 0.5 M EDTA (pH 8.0). After the addition of 0.1 volume of 5 M sodium chloride and 3 vol. of cold 100% ethanol, RNAs were ethanol precipitated at –20°C overnight and then purified by electrophoresis on urea-containing polyacrylamide denaturing gels using a DNA sequencing system (JY-CX2B from BEIJING JUNYI Electrophoresis Co., Ltd.) at 120 W. The gel bands were visualized by UV-shadowing, and excised from the gel. Then the RNAs were eluted using the Elutrap Electroelution System (GE Healthcare) at 150 V overnight. All purified RNAs were washed with 2 M NaCl, and then desalted and exchanged extensively into an NMR buffer using an appropriate Amicon Ultra Centrifugal Filter Device (Millipore).

To investigate the heterodimer formation of DsrA32 and rpoS25 by NMR, equal amounts of DsrA and rpoS were mixed to give a final concentration of 1.2 mM of total RNA. The samples were incubated at 95°C for 5 min and

then slowly cooled to room temperature. RNA sample concentrations were determined by measuring the optical absorbance at 260 nm.

Gel mobility shift assays

The DsrA32/rpoS25 binding assay was performed in a 10 μl reaction mixture in NMR1 buffer (10 mM sodium phosphate at pH 6.5 and 50 mM NaCl). DsrA32 and rpoS25 samples were prepared at 20 μM stock solutions in NMR1 buffer. Then, 0, 0.5 and 1 μl rpoS25 was added to 1 μl DsrA32 to give 0:1, 0.5:1 and 1:1 rpoS25:DsrA32 ratios, respectively. The reactions were incubated at 95°C for 5 min and then slowly cooled to room temperature. After the addition of 2 μl 80% glycerol, the samples were resolved on 0.5 × Tris-borate buffer (50 mM Tris base, 50 mM boric acid) 10% native 19:1 polyacrylamide gels. Gels were stained with Gel-Red, and photographed with a gel imaging system.

Binding reactions between the mRNAs and the SL12 wild type (WT) or SL12 ΔC53 mutant were performed in a 10 μL reaction mixture containing 10 mM sodium phosphate, pH 6.5, and 2 mM $MgCl_2$. The SL12 WT and SL12 ΔC53 mutant were prepared at 1 μM stock solution in NMR2 buffer (10 mM sodium phosphate at pH 6.5). Prior to use, they were refolded by heating for 1 min at 90°C and incubating on ice over 5 min. The lyophilized RNA oligomers (rpoS18 and R22 RNAs) labeled at their 5′-termini with Carboxyfluorescein (FAM) were obtained from Takara Bio, Inc., and dissolved in diethylpyrocarbonate (DEPC)-treated water to a final concentration of 100 μM. Before the binding reaction, they were diluted to 2 μM in NMR2 buffer. The final concentration of FAM-labeled RNAs was 200 nM, and the final concentrations of the SL12 WT and SL12 ΔC53 RNAs were as indicated (Figure 7). Reactions were incubated on ice for 20 min. Prior to gel loading, the binding reactions were mixed with 2 μl of native loading buffer (80% glycerol, 0.02% (w/v) bromophenol blue), and the samples were loaded onto 10% native 19:1 polyacrylamide gels in 0.5 × TB buffer with 2 mM $MgCl_2$. Gels were run on ice at 150 V for 30 min and scanned using a Typhoon FLA 7000 (GE Healthcare). Each experiment was performed on the same gel and was repeated at least three times.

Multi-angle light scattering

Size exclusion multi-angle light scattering (SEC-MALS) data was collected using an ÄKTA pure system (GE Life Sciences) with a Superdex 200 Increase 10/300 GL column (GE Life Sciences) at a flow rate of 0.75 ml/min in running buffer (10 mM sodium phosphate at pH 6.5 and 100 mM NaCl). The system was coupled on-line to an 18-angle MALS detector (DAWN HELEOS II, Wyatt Technology) and a differential refractometer (Optilab T-rEX, Wyatt Technology). Molar mass determination was calculated using ASTRA 7.0.1.24 software.

NMR spectroscopy and signal assignments

For NMR studies, $SL1_{+4}$ was prepared in NMR1 buffer, while the other RNA samples were prepared in NMR2 buffer. NMR spectra were recorded on Bruker DMX 600 MHz, AVANCE III 900 MHz and Agilent 700 MHz spectrometers equipped with HCN cryoprobes at 283 K for exchangeable and at 303 K for non-exchangeable proton spectra.

To determine the solution structure of $SL1_{+4}$, 2D NOESY (mixing time = 200 ms), 2D ^{1}H–^{15}N HSQC, 2D H6/H5(C4N)H (38) and 3D ^{1}H–^{15}N NOESY-HSQC spectra in 90% H_2O/10% D_2O, recorded with unlabeled and uniformly ^{13}C,^{15}N-labeled samples, were obtained to unambiguously assign the imino and amino exchangeable protons. RNA base pairs were confirmed with 2D HNN-COSY experiment. Assignments for all non-exchangeable protons were obtained from 2D NOESY (mixing time = 250 ms), 2D ^{1}H-^{13}C HSQC, 2D TOCSY, 2D HCN, 3D HCCH-COSY, 3D HCCH-TOCSY and 3D ^{1}H-^{13}C NOESY-HSQC datasets in D_2O. The sugar pucker was determined with 2D DQF-COSY. Imino proton resonance assignments of other RNAs were obtained by standard sequential assignment methods in 2D NOESY. All NMR data were processed using NMRPipe/NMRDraw and analysed using Sparky and NMRView.

Structure calculations

Initial structures of $SL1_{+4}$ were calculated with CYANA 3.0 by adding the manually assigned NOEs. Upper distance limits of 2.7, 3.3, 5.0 and 6.0 were generally employed for cross-peaks of strong, medium, weak and very weak intensity, respectively. Standard hydrogen-bonding restraints for all nine base pairs were employed, and cross-helix phosphate-phosphate distance restraints (with a 20% weighting coefficient) were used in the helical segments to limit the approach of the phosphate groups. Torsion-angle restraints were used for the nucleotides of standard A-form geometry, allowing for ±25° deviations from ideality ($\alpha = -62°$, $\beta = 157°$, $\gamma = 48°$, $\delta = 83°$, $\epsilon = -152°$, $\zeta = -73°$). Nucleotides U13-C15 with observable H1'-H2' and H1'-H3' correlations were constrained as C2'-*endo* (South; $\delta = 142.5° \pm 37.5°$). Except for δ, no torsion angle restraints were applied for U13-C15 in the loop. The 20 CYANA-minimized structures with the lowest target function were refined in the ff99bsc0_chiOL3 force field using the sander module of AMBER14 using a protocol as previously described (39). The statistics table for the $SL1_{+4}$ structure ensemble is included in Supplementary Table S2. Molecular images were generated using PyMOL (http://www.pymol.org).

RESULTS

DsrA-SL1 forms a stable A-form helix capped by a dynamic pentaloop

As an ∼90-nucleotide non-coding RNA, the full-length DsrA is extremely challenging for solution NMR studies. Therefore, we adopted a divide-and-conquer approach to investigate the individual stem–loops and then validated the results in the context of the full-length sequence. The wild-type sequence of DsrA-SL1 (SL1 WT) includes the nucleotides from 4 to 22, with a G19•U7 wobble base pair

and a capping AUUUC pentaloop. To determine the solution structure of SL1, we prepared a 23-nucleotide $SL1_{+4}$ RNA, with two non-native G–C base pairs added at the end of the helical stem to generate a high level of RNA transcription (Figure 2A). Using a combination of homonuclear and heteronuclear 2D and 3D NMR experiments on unlabeled or uniformly ^{13}C,^{15}N-labeled samples in H_2O and D_2O, almost complete ^{1}H and protonated-^{13}C and -^{15}N signals were assigned.

Assignments were made for all guanine and uracil imino proton signals observed at 10°C, except for the nucleotides in the loop region (U12, U13 and U14), using 2D NOESY and 2D HNN-COSY. Figure 2B shows the imino proton resonances in 1D NMR spectrum and the base pairs between imino protons and their hydrogen-bonded nitrogen atoms in 2D HNN-COSY. Sequential assignment of the aromatic H6/H8 protons to the ribose H1' proton indicates that $SL1_{+4}$ forms an A-form helix from G-2 to G10 and from C16 to U22 (Figure 2C). In the pentaloop, the sequential base-H1' connectivity can be observed from G10 to A11. A11-H2 has NOEs with U12-H1' and C16-H1' and the A11-H8 proton has a strong NOE cross-peak with G10-H2' (Figure 2D), indicating that A11 actually stacks on G10. In addition, weak NOEs are observed between U12-H6 and A11-H1'/H2' when A11-H8 also exhibits an NOE with U12-H5. These results indicate that U12 stacks on A11, but this stacking does not deviate from standard A-form geometry. No NOE connectivity from U12 to C16 is observed in both 2D NOESY and 3D ^{1}H-^{13}C NOESY-HSQC (Figure 2D). Due to the absence of the H1'-H2' cross-peak in the 2D ^{1}H-^{1}H DQF-COSY spectrum, all the nucleotides in the stem plus A11 should adopt a C3'-*endo* A-form sugar pucker conformation (Supplementary Figure S1). U12 has a H1'-H2' cross peak with a J-coupling constant of 7.2 Hz, indicating that U12 ribose is in a conformational equilibrium between C2'- and C3'-*endo* character. Three other nucleotides in the loop (U13, U14 and C15) all have a coupling constant larger than 9 Hz, suggesting a significant C2'-*endo* conformation for their riboses, which is further confirmed by the strong intra-nucleotide H6-H2' NOEs relative to H6-H3'. All these data indicate that there is no base-stacking from U12 to C16, and their structures are highly dynamic and disordered.

The solution structure of $SL1_{+4}$ was finally solved by using 397 NOE distance restraints for an average of 17 NOE restraints per nucleotide and 21 total restraints per nucleotide (Supplementary Table S2). The superposition of the 20 lowest energy structures was performed over all heavy atoms yielding an RMSD to the mean of 1.87 Å for all heavy atoms in SL1 and 0.17 Å for heavy atoms in the stem region (Figure 3A). The structure of $SL1_{+4}$ is well defined, with a regular A-form helix capped by a dynamic pentaloop in which all nucleotides in the stem are base paired and stacked in the helix (Figure 3B). The overall orientation of the AUUUC pentaloop of DsrA-SL1 is very similar to the AUGUG pentaloop of 7SK-SL4 (Supplementary Figure S2): the first two nucleotides in the 5′-side of the loop are stacked in a helical environment while the next three nucleotides in the 3′-side loop are highly flexible (Figure 3C) (40).

rpoS mRNA unwinds DsrA-SL1 and DsrA/*rpoS* forms an A-form duplex

Previous RNA footprinting analysis has shown that DsrA-SL1 and Linker1 bind to the 5′ UTR region of *rpoS* mRNA accompanied by the unwinding process of DsrA-SL1, which will in turn release the ribosome binding site on *rpoS* (21). To investigate the details of this interaction, we designed a DsrA32 RNA (nucleotides from 1 to 32 of DsrA) and a rpoS25 RNA (nucleotides from –119 to –95 of *rpoS*) for further biochemical and NMR studies (Figure 4A). To test the binding, we incubated the DsrA32 and rpoS25 RNAs together at 95°C for 5 min and then slowly cooled down to room temperature. The native PAGE experiment showed that addition of rpoS25 to DsrA32 led to a distinct, stoichiometric band shift (Figure 4B), indicating that DsrA32 and rpoS25 formed a stable heterodimer at 1:1 ratio. No additional bands were observed at DsrA32/rpoS25 heterodimer ratios above 1:1.

Although a DsrA32/rpoS25 heterodimer is obtained, its NMR signals assignment turns out to be very difficult due to the heavy resonance overlap and weak cross-peaks. To study the structure of DsrA32/rpoS25 complex, we prepared four new RNA samples (R58, R58L, R58M and R58U) (Figure 4A). R58 RNA contains the intact stem region of DsrA32/rpoS25 complex and is capped by a GGAA tetraloop (a member of the well-characterized GNRA family). R58L, R58M and R58U RNAs are derived from the lower stem, middle stem and upper stem of the R58 RNA, respectively. 1D ^{1}H spectra and 2D ^{1}H–^{1}H NOESY spectra were performed for all RNA constructs in H_2O, while 2D ^{1}H–^{1}H NOESY and 2D ^{1}H–^{1}H DQF-COSY spectra were collected for R58, R58L, R58M and R58U RNAs in D_2O.

Those imino protons, which belong to the central base pairs within a stretch of the same three adjacent base pairs, have almost the same chemical shift (Figure 4C) and identical NOE cross-peak patterns within all RNA constructs. For example, DsrA32/rpoS25 heterodimer and R58 RNA have an almost same imino NOE cross-peak patterns, except the first base pair and the last two base pairs of the stem region of DsrA32/rpoS25 heterodimer (Supplementary Figure S3A). In the absence of two non-native G-C base pairs and a GGAA tetraloop, the imino proton signals of three above-mentioned base pairs in DsrA32/rpoS25 heterodimer are strongly attenuated by fast water exchange and therefore undetectable in the NOESY experiment. With the help of the assignments of R58L, R58M and R58U RNAs, the imino proton resonances of R58 (Supplementary Figure S3B) and DsrA32/rpoS25 heterodimer (Figure 4D) were unambiguously assigned, except several missing signals in the middle bulge (G18, G19, U20, G-105). These results indicated that the stem region of DsrA32/rpoS25 heterodimer had the same structure as R58 RNA, which contains stable lower and upper stems with a dynamic bulge in the middle region.

Sequential assignment of the aromatic H6/H8 protons to the ribose H1' proton in 2D NOESY indicates that the A-form helix is formed in both R58L and R58U (Supplementary Figure S3C and S3D). The absence of H1'-H2' couplings and strong (*n*)H6/H8 to (*n* – 1)H2' NOEs also indicate that R58L and R58U RNAs have retained the

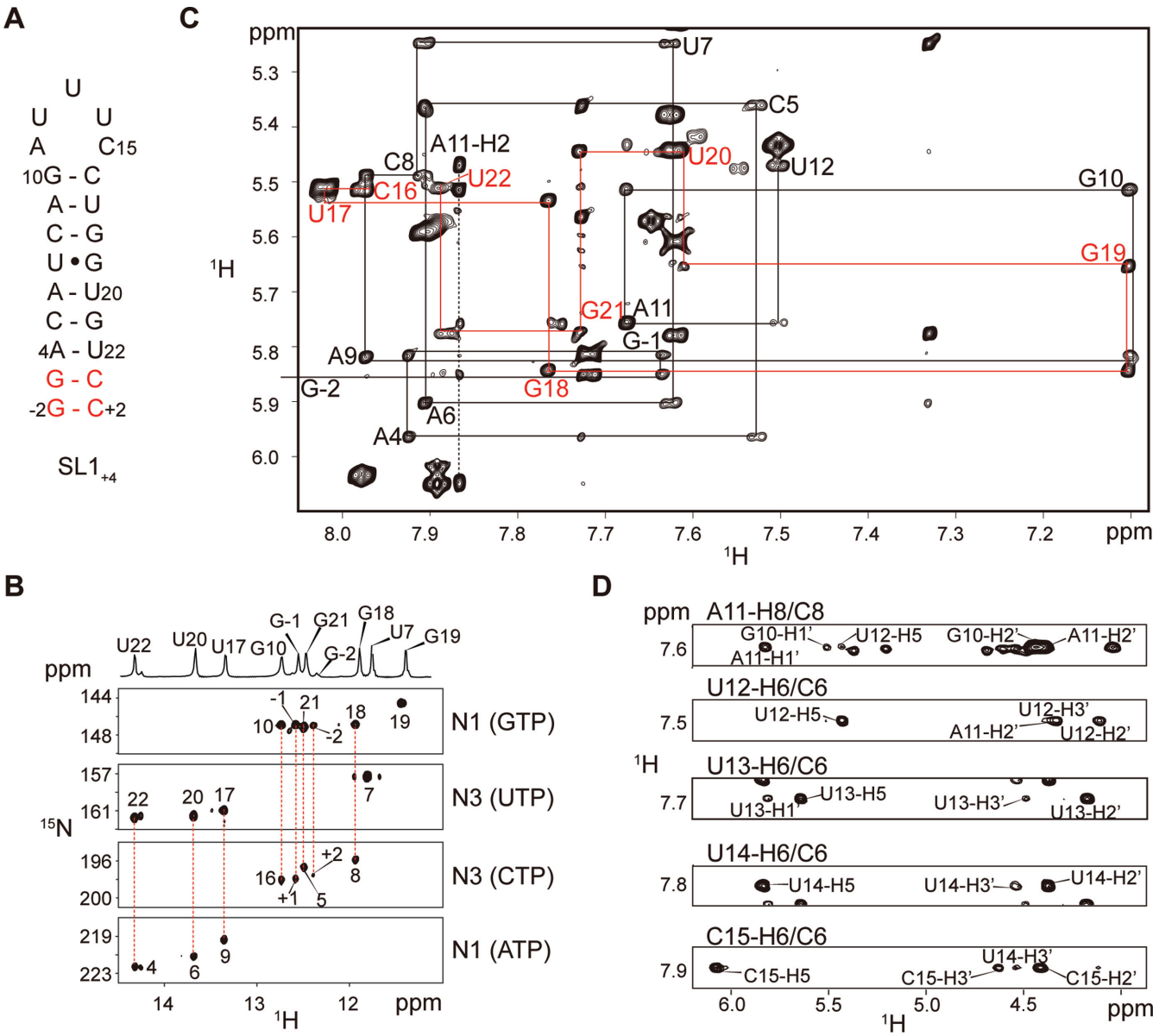

Figure 2. Representative NMR spectra collected for $SL1_{+4}$. (**A**) Secondary structure of SL1. $SL1_{+4}$ is the construct derived from the wild-type (SL1 WT, residues 4–22) and used for structural determination by NMR. Two nonnative G–C base pairs (colored in red) are added to the SL1 WT to increase the yield of RNA transcription. (**B**) Imino proton region of 1D NMR spectrum and 2D ^{1}H–^{15}N HNN-COSY reveals the base pairs of $SL1_{+4}$. Imino protons and their hydrogen-bonded nitrogen atoms in the canonical base pairs are shown in red bash lines. In HNN-COSY, the cross-peaks are labeled by the residue number. (**C**) Portion of 2D NOESY spectrum obtained for unlabeled $SL1_{+4}$ showing cross-peaks between aromatic H6/H8 protons and ribose H1' protons. Sequential NOE connectivities are indicated with lines. The base-H1' sequential walk is traced in black on the 5′-half (G-2 to U12), red on the 3′-half (C16 to U22) and a black dashed line on A11-H2. G-2 falls outside the spectral region shown. The cross-peaks are labeled with the one-letter nucleotide code and the residue number. (**D**) Expansion of planes corresponding to C6/C8 regions of the loop residues A11 to C15 taken from 3D ^{1}H–^{13}C NOESY-HSQC spectrum collected from uniformly ^{13}C,^{15}N-labeled $SL1_{+4}$. Unlabeled peaks are due to partially overlapping resonances from other spin systems.

C3'-*endo* conformation. Moreover, similar NOE patterns of adenosine-H2 to ribose-H1' signals were observed for R58, R58L and R58U (Figure 4E), indicating that the lower and upper stems of R58 form the same A-form helix structures as R58L and R58U, respectively.

DsrA-SL1 forms a very stable hairpin structure, and has the same imino proton resonances in DsrA32 (Figure 4C) and $SL1_{+4}$ (Figure 2B) RNAs. However, these signals disappeared in the DsrA32/rpoS25 heterodimer. Taken together, all these results indicated that DsrA-SL1 is unwound upon the binding with *rpoS* and the DsrA/*rpoS* complex forms an A-form duplex in the lower and upper stems plus a dynamic bulge. Note that the DsrA-SL1 unwinding won't happen if DsrA32 is incubated with rpoS25 RNA at room temperature (data not shown), suggesting that the DsrA-SL1 unwinding and the DsrA/*rpoS* duplex formation may not happen spontaneously and needs the assistance of some other factor(s) *in vivo*.

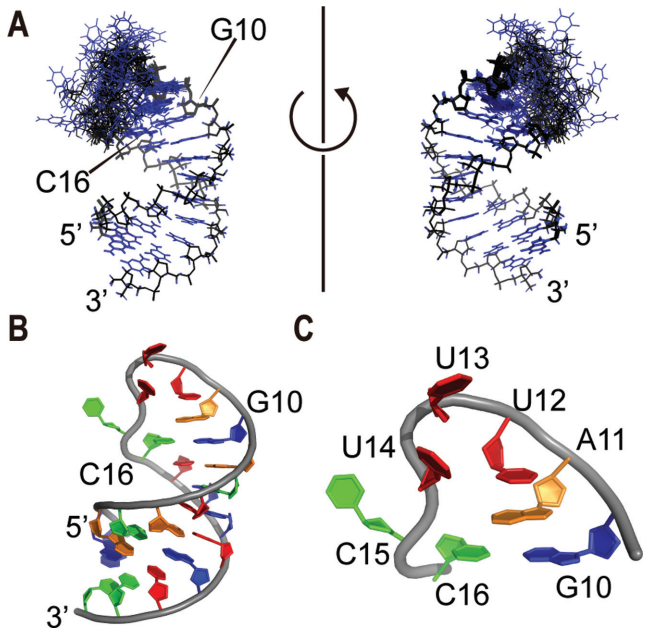

Figure 3. NMR solution structure of $SL1_{+4}$. (**A**) Superposition of the 20 lowest energy structures. The base and ribose are colored blue and black, respectively. (**B**) The lowest-energy structure of $SL1_{+4}$ represented as a ribbon-and-stick model. Nucleotides are colored blue (guanosine), green (cytosine), orange (adenine) and red (uracil). (C) Close-up views of the AUUUC pentaloop.

Secondary structure of DsrA-SL2

Four distinct secondary structure models of DsrA (Models A–D) have been previously proposed (Supplementary Figure S4). All these models shared the same SL1 and SL3, but a variable organization for the nucleotides 23–60 (including Linker1 and SL2, named Domain2). To verify the secondary structure of SL2 in NMR condition, several DsrA constructs were transcribed (Figure 5A), including the 89-nt full-length (the sequence derived from (41)), SL12 (nucleotides 1–60, SL1-Linker1-SL2), Domain2 (nucleotides 23–60, Linker1-SL2), SL23 (nucleotides 35–87, SL2-linker-SL3), $SL2_{+4}$ and $SL3_{+4}$ (Figure 5A). $SL2_{+4}$ has the same sequence as the Model B with two additional G-C base pairs at the open end of the stem.

We first assessed the folding of $SL2_{+4}$ and Domain2 by comparing their 2D ^1H–^1H NOESY spectra (Supplementary Figure S5A). Because $SL2_{+4}$ does not seem to exist as a monomer in NMR buffer (Supplementary Figure S5B and S5C), its NMR resonances of $SL2_{+4}$ are much weaker than those of Domain2. Even though, all the strong imino resonances belonging to the upper stem of SL2 have identical chemical shift and the NOE cross-peak patterns in these two RNAs, suggesting that SL2 maintain the same conformation in $SL2_{+4}$ and Domain2, and the 13-nt Linker1 does not participate into the formation of the hairpin structure. To verify whether the structures of the SL1 and SL2 subdomains are maintained in the context of the SL12 RNA, we investigated the base pairing of SL12 by NMR (Supplementary Figure S5D). Imino proton resonances were identified with cross-peak patterns and chemical shifts corresponding to those observed for SL1 and Domain2 RNAs, indicating that the structures of these subdomains were present in the context of SL12. On the same account, the structures of SL2 and SL3 were present in the context of SL23 (Supplementary Figure S5F). As SL23 only contains the sequences from the first nucleotide A35 of SL2, this also indicates that the region of nucleotides A23-U34 is a single strand linker.

Because of the better resolution and signal-to-noise ratio, Domain2 RNA was further used to study the secondary structure of SL2. The Watson–Crick and G•U wobble base pairs were identified from the NOEs of imino–to-imino (Figure 5B), imino-to-aromatic and imino-to-amino protons in 2D ^1H–^1H NOESY (Supplementary Figure S5E). The upper stem shows sequential imino to imino cross-peaks from the C40–G56 base pair to U42–A54 base pair and from C43–G52 base pair to U45–A50 base pair. Due to the existence of a single-nucleotide bulge (C53), the NOE between G52–H1 and U42–H3 is missing. And the imino proton resonance of U41 overlaps with G52 at 10°C. Consistent with the above-mentioned model B, G37•U57 wobble base pair and two A–U base pairs form the lower stem, which is separated from the upper stem by two unpaired nucleotides (U38 and G39). The imino protons of G37•U57 can be unambiguously assigned based on their characteristic chemical shifts and the strong NOE between these two imino protons in the 2D NOESY. However, no further imino-to-imino cross-peak between G37•U57 and other base pair is observed, suggesting a structural instability for the lower stem. Note that the imino resonance of U58 was assigned by using its NOE with A36-H2 in $SL2_{+4}$, Domain2 and SL23 RNAs. All the assignments were checked in the region of imino-to-aromatic and imino-to-amino (Supplementary Figure S5E). In summary, our NMR analysis exhibits a secondary structure of SL2 in Domain2 RNA which is highly similar to that in model B, including that the lower stem stem is as unstable as proposed (Figure 5C).

While comparing the imino proton resonances of three stem–loops in SL12 (Supplementary Figure S5D) and SL23 (Supplementary Figure S5F), we found that the imino protons belonging to Domain2 experienced exchanged line-broadening and were much weaker than those in SL1 and SL3. And in the 2D ^1H–^1H NOESY of Domain2 RNA, strong sequential imino-to-imino walks in the upper stem were observed, but not in the lower stem. Thus, these NMR data are consistent with the previous ribonuclease footprinting results (21), suggesting that the upper stem of SL2 is unstable and the lower stem is much more flexible.

Two conformational states of DsrA-SL2

It has been indicated that, upon the binding with mRNA, the Linker1 and the lower stem of SL2 of DsrA can form duplex with mRNA (42). To study the remaining structure of SL2 after binding, we generated several RNA constructs of Domain2 with the stepwise deletion of the region that can interact with different mRNAs, including $Domain2_{35nt}$ (nucleotides 28–60), $Domain2_{30nt}$ (nucleotides 33–60), $Domain2_{25nt}$ (nucleotides 38–60) and $Domain2_{20nt}$ (nucleotides 43–60) (Figure 6B). These different constructs are expected to mimic the remaining structures of DsrA after base-pairing with different mRNAs.

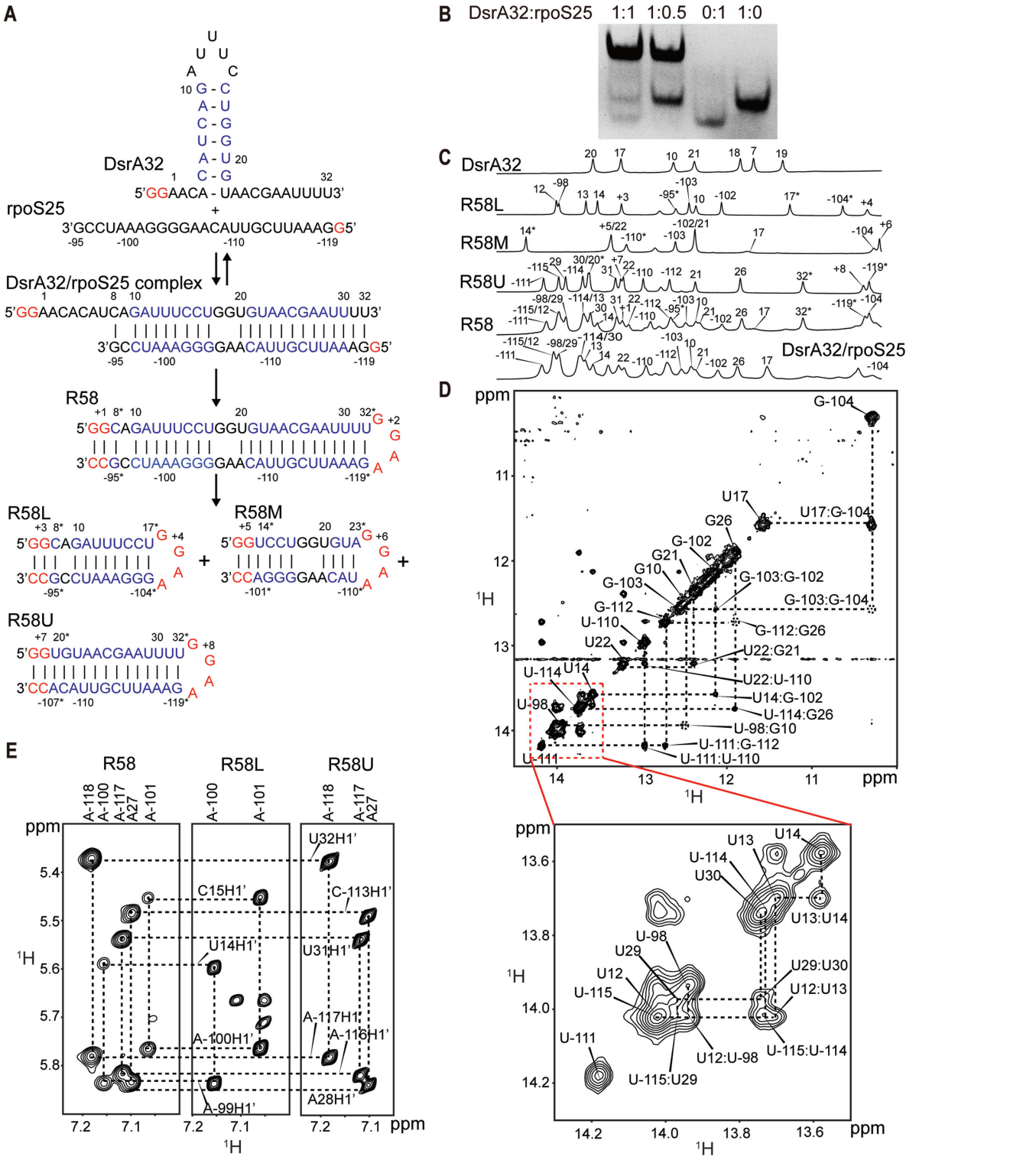

Figure 4. Translation regulation of *rpoS* by DsrA. (**A**) RNA constructs used in the present studies. DsrA32 includes nucleotides from 1 to 32 of DsrA, and rpoS25 includes nucleotides from –119 to –95 of *rpoS*. R58L, R58M and R58U RNAs are derived from the lower stem, middle stem and upper stem of the R58 RNA, respectively. The red letters indicate non-native nucleotides; the blue letters indicate base pairs of which imino proton resonances were observed and assigned in 2D ^{1}H–^{1}H NOESY spectra. The nucleotides with different adjacent nucleotides from DsrA32/rpoS25 complex are labeled by stars. (**B**) Native PAGE shows that DsrA32 and rpoS25 form a stable heterodimer at 1:1 DsrA32:rpoS25 molar ratios. (**C**) 1D imino proton spectra of the RNA constructs. From top to bottom are free DsrA32, R58L, R58M, R58U, R58 and DsrA32/rpoS25 complex, respectively. The assignments of all RNA constructs are labeled by the sequence number. (**D**) Imino proton region of the NOESY spectrum (in 90% H_2O/10% D_2O) of DsrA32/rpoS25 complex recorded at 900 MHz spectrometer. (**E**) Portions of the 2D NOESY spectra (in 100% D_2O) showing the cross-peaks of adenosine-H2 and ribose-H1' observed for (from left to right) R58, R58L and R58U RNAs. Adenosine-H2 and ribose-H1' assignments are labeled vertically and horizontally, respectively.

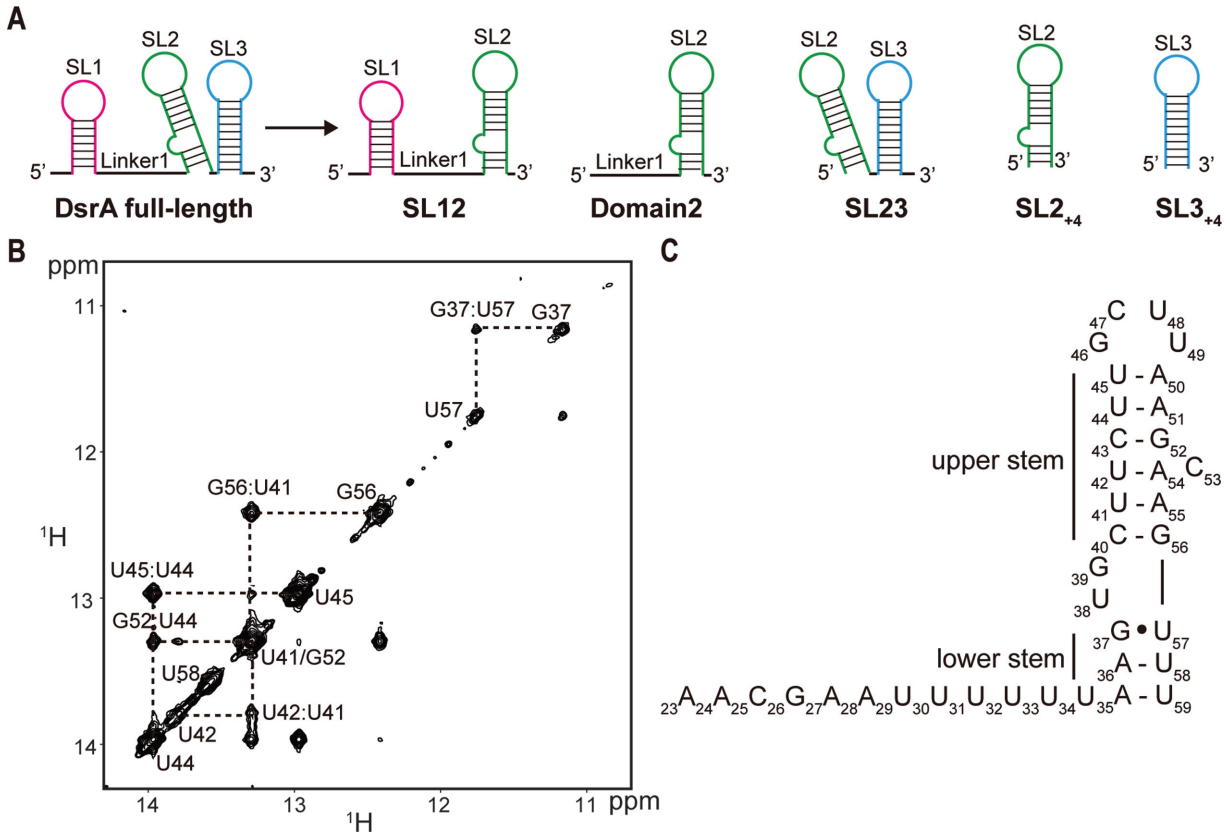

Figure 5. NMR studies of DsrA-Domain2. (**A**) The constructs of DsrA used for this study. SL1, SL2 and SL3 are colored magenta, green and cyan, respectively. From the left, DsrA full-length, SL12, Domain2, SL23, $SL2_{+4}$ and $SL3_{+4}$. Two nonnative G–C base pairs are added to the SL2 and SL3. (**B**) Portion of 2D ^{1}H–^{1}H NOESY spectrum of Domain2. (**C**) Secondary structure of Domain2 derived from NMR spectra.

Intriguingly, in the 2D ^{1}H–^{1}H NOESY in H_2O, we observed the existence of two conformers of SL2, named Fold A and B (Figure 6A). In the 2D NOESY spectrum of Domain2 (Figure 5B), all cross-peaks of the imino proton resonance are the same as those in Fold A. For $Domain2_{35nt}$, it lacks the first five nucleotides of the linker of Domain2, however, most of its cross-peaks are similar to those in Fold B. Only weak G37:U57 and U45:U44 cross-peaks maintain their chemical shifts as in Fold A (Figure 6C, top left). The imino-to-imino cross-peak of U45:U44 of Fold A is the most intense peak in the upper stem of SL2, so it can be observed while others are not. This result indicates that a large population of $Domain2_{35nt}$ adopts Fold B, while a minor portion of RNA adopts Fold A. Meanwhile, the intensities of the cross-peaks that belongs to Fold B are still weak. For example, the NOEs from the imino proton of G56 to the imino protons of U42 and U57 in $Domain2_{35nt}$ cannot be observed. These results suggest that Fold B of SL2 in $Domain2_{35nt}$ RNA is unstable and may be easy to unwind.

Interestingly, in $Domain2_{30nt}$, which contains almost the same sequence as SL2, the population ratio of Fold A to Fold B was almost inversed when comparing with $Domain2_{35nt}$. All the cross-peaks of Fold A plus the U42:U57 and G52:G46 cross-peaks from Fold B can be observed for this RNA (Figure 6C, top right). Furthermore, in $Domain2_{25nt}$ which is predicted to fold as in Figure 6B, the same populations of Fold A and B are mostly observed (Figure 6C, bottom left). The imino proton resonances of $Domain2_{25nt}$ were confirmed by 2D ^{1}H–^{15}N HSQC using uniformly ^{15}N-labeled sample (Supplementary Figure S6A). Finally, in the shortest construct $Domain2_{20nt}$, which lacks an intact upper stem of Fold A, only the resonances of Fold B were observed (Figure 6C, bottom right). Therefore, the 2D NOESY spectra unequivocally confirmed the existence of two conformers of SL2, and Linker1 and the unstable lower stem of SL2 affected their equilibrium.

To investigate the conformational exchange process between two different folds, a 2D ^{1}H-detected ^{15}N exchange spectroscopy (EXSY) with a mixing time $\tau_m = 1.2$ s was performed on ^{15}N-labeled $Domain2_{25nt}$ RNA (Supplementary Figure S6B). Only very weak cross-peaks of two imino proton (G52 and U45) from Fold B to Fold A were observed, while no obvious cross-peak from Fold A to Fold B was detected. This result suggests that the conformational exchange from Fold B to Fold A is in the subsequent time-interval $\tau_m = 1.2$s.

Conformational flexibility makes DsrA more accessible to multiple target mRNA binding

To investigate the role of conformational flexibility of DsrA in multiple target mRNA regulation, we studied the binding affinities of DsrA and mRNAs. In SL2, C53 forms a single-nucleotide bulge in the Fold A conformation, but participates in the base-pairing in the stem region of Fold B con-

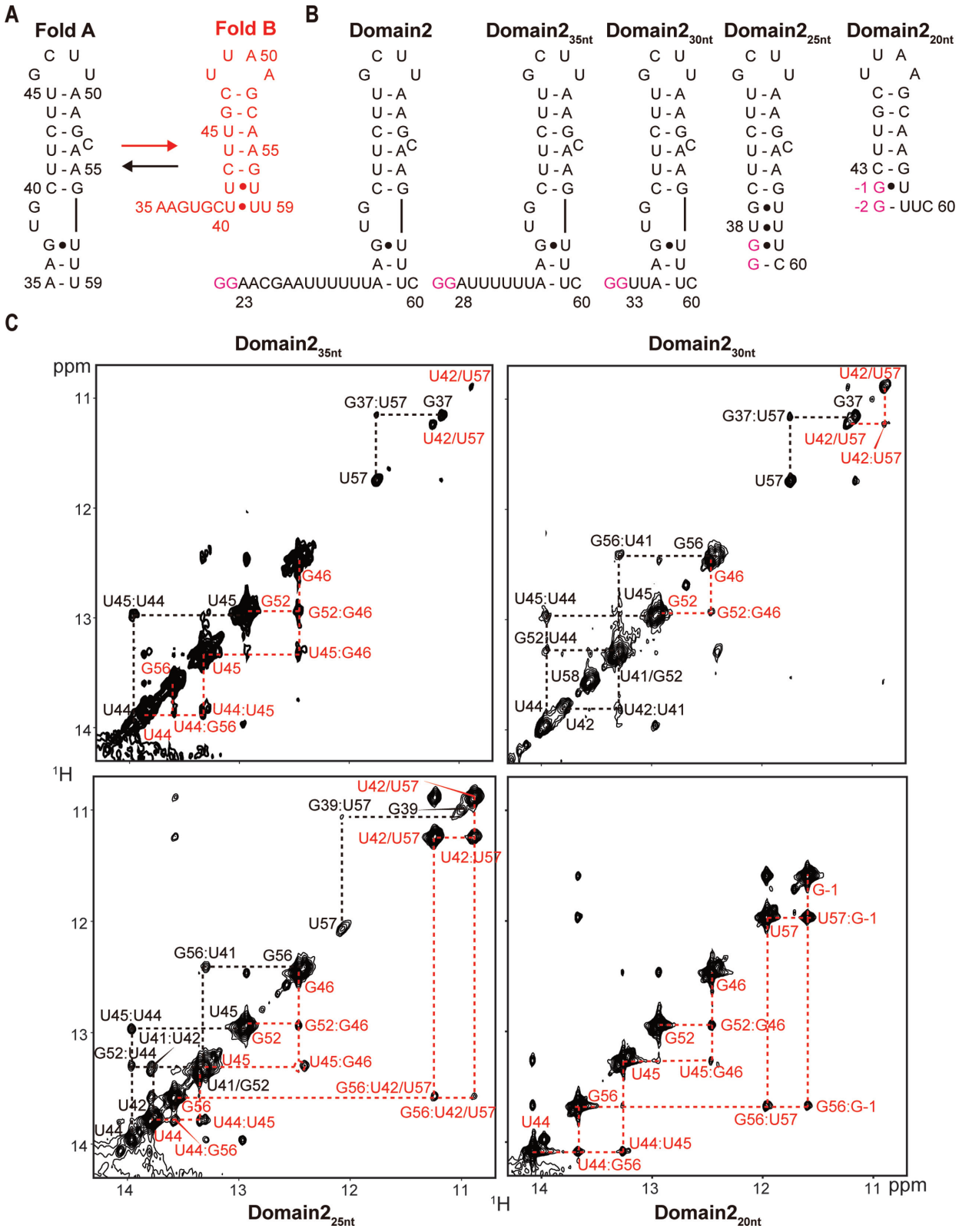

Figure 6. Bistable structure of SL2. (**A**) Schematic of bistable secondary structures of SL2. Nucleotides of Fold A are colored black, and Fold B are colored red. (**B**) RNA constructs used in the present studies. Non-native nucleotides are shown in magenta. (**C**) Imino-to-imino NOEs cross-peaks of Domain2$_{35nt}$ (top left), Domain2$_{30nt}$ (top right), Domain2$_{25nt}$ (bottom left), Domain2$_{20nt}$ (bottom right) with color-coded signal assignments.

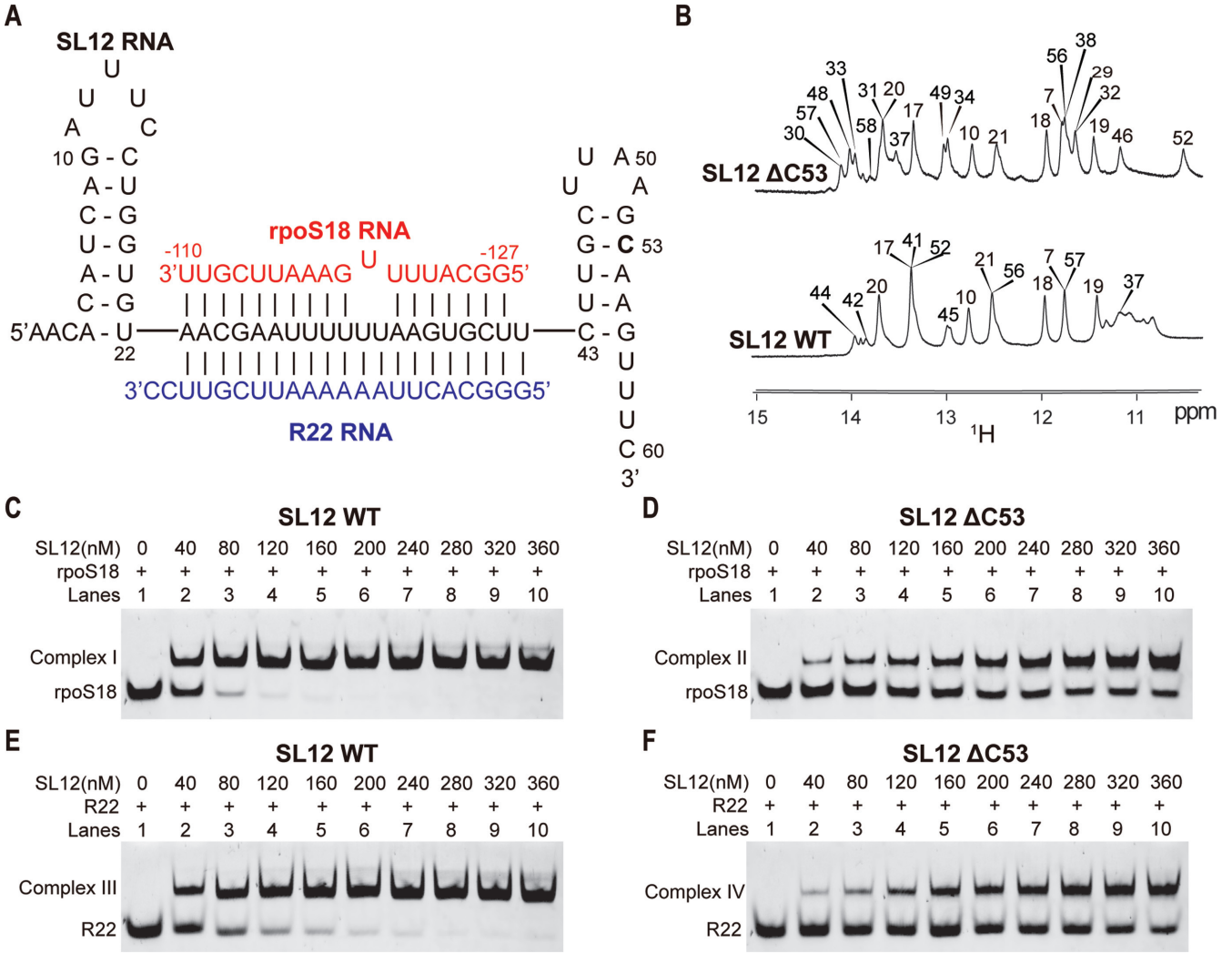

Figure 7. The effects of DsrA structure on mRNAs binding affinities. (**A**) Schematic of the RNA constructs used for this study. SL12 RNA contains the first two stem–loops of DsrA (nucleotides 1–60). C53 is labeled in bold letter and the residue number. SL12, rpoS18 and R22 RNAs are colored black, red and blue, respectively. (**B**) 1D imino proton spectra of SL12 ΔC53 mutant (top) and SL12 wild type (WT) (bottom). Imino proton resonances are labeled by the residue number. Using gel mobility shift assays, *in vitro* binding of rpoS18 RNA and SL12 WT (**C**) or ΔC53 mutant (**D**) was performed as described in Materials and Methods. 200 nM of 5′-FAM-labeled rpoS18 RNA was incubated with increasing concentrations of unlabeled SL12 WT or ΔC53 mutant (final concentrations above the lanes). Following 20 min incubation on ice, samples were run on a native 10% gel. The same experimental procedure as above but with 5′-FAM-labeled R22 RNA and increasing concentrations of unlabeled SL12 WT (**E**) or ΔC53 mutant (**F**).

formation (Figure 7A). In addition, this single-nucleotide bulge also exists in the proposed Model A for DsrA secondary structure (Supplementary Figure S4A). To study whether the existence of C53 will influence the dynamic conformational equilibrium of DsrA RNA, we generated a C53-deleted mutant from SL12 (SL12 ΔC53). Interestingly, in this SL12 ΔC53 mutant, SL2 forms a new secondary structure (called Fold C), which has a much longer stem than Fold A and Fold B as suggested by imino-to-imino NOE connectivities (Supplementary Figure S7A and S7B). On the other hand, SL12 wild type (SL12 WT) and SL12 ΔC53 mutant maintain the same imino proton resonances of SL1 (Figure 7B), indicating that the C53 deletion does not change the structure of SL1. Fold C has the same secondary structure as the SL2 in Model A except for the bulge nucleotide C53, and it contains only three nucleotides in the linker region between SL1 and SL2.

To investigate whether the C53 deletion affects the binding affinities between DsrA and its target mRNAs, two 5′-FAM-labeled RNA oligomers (rpoS18 and R22) were designed for binding assay with the SL12 WT and ΔC53 mutant (Figure 7A). The sequence of rpoS18 RNA comes from the 5′-UTR of *rpoS* mRNA (nucleotides from –127 to –110), and is predicted to base pair with DsrA from residue A23 to U41 using the isoenergetic microarray mapping method (32). It has been reported that the DsrA sequence of A23 to U42 can not only base pair with *rpoS* mRNA, but also with *hns* and *mreB* mRNAs (Supplementary Figure S8) (42,43). R22 RNA was therefore designed to completely base pair with the above nucleotides of DsrA except the last two cytosines at the 3′ terminal. The bind-

ing assay was performed at a concentration range of 0–360 nM for both the SL12 WT and the ΔC53 mutant. When 120 nM SL12 WT is present, almost all the 200 nM rpoS18 RNA forms a SL12/rpoS18 complex (Complex I) (Figure 7C). However, even at the highest concentration of 360 nM for the ΔC53 mutant, there remains many free rpoS18 (Figure 7D). We also observed reduced binding affinity of R22 RNA for the ΔC53 mutant (Figure 7F) compared to the SL12 WT (Figure 7E). As C53 is not involved in the direct base-pairing with *mreB*, *hns* or *rpoS* mRNAs (Supplementary Figure S8), all these data indicate that conformational plasticity makes DsrA more accessible to mRNA binding and plays a potentially important role in its multiple target regulation.

NMR structural study of the full-length DsrA

Although the structure of SL2 is dynamic, the resolutions of the 2D NOESY spectra of both SL12 and SL23 are quite good, probably because both these RNA constructs contain two stem–loops. Thus, NMR was further employed to investigate whether the full-length DsrA could form a three stem–loop structure in solution. Unexpectedly, 1D ^{1}H spectrum and 2D ^{1}H-^{1}H NOESY showed that all the strong imino proton resonances of the full-length DsrA and their NOE patterns are consistent with those of SL1 even at a low concentration (20 μM) (Figure 8A and B). Increasing the temperature or adding magnesium did not cause the appearance of more imino peaks (data no shown). Next, we compared the H5-H6 cross-peaks of uracil and cytosine between SL1 and the full-length RNA in 2D ^{1}H–^{1}H TOCSY spectra (Figure 8C). Except two manually added cytosines at the 3′-end and U22 which has a different chemical shift, other nucleotides of SL1 show almost the same chemical shift in the two RNAs. Those H5–H6 cross-peaks belonging to SL1 have better chemical shift dispersion, sharper line width and higher intensity than other cross-peaks in the TOCSY spectrum of the full-length RNA. Although there are total 49 nucleotides of uracil and cytosine in the full-length RNA, only approximately 22 H5–H6 cross-peaks with good resolution were observed in the TOCSY spectrum (Figure 8D), indicating that most of the H5-H6 resonances from SL2 and SL3 do not have good dispersion chemical shift and/or intensity. To better understand the structure of the full-length DsrA, we performed SEC-MALS experiment (Figure 8E). At 20 μM (0.58 mg/ml), the full-length DsrA eluted as a wide peak, indicative of a broad distribution of oligomeric states with an average mass of 97 kDa (3–4 DsrA monomers, expected mass of 29 kDa for one monomer). Taken together, these data suggest that the full-length DsrA forms oligomeric states at high concentration, and only SL1 maintains an A-form hairpin structure.

DISCUSSION

Although the involvement of DsrA sRNA in the regulation of several mRNAs has been identified and four different secondary structures of DsrA have been proposed, no atomic resolution structures of DsrA have been so far reported. As the first step toward the characterization of the complex structure of the DsrA/mRNA and the understanding how DsrA base pairs with different mRNAs and regulates their translation mediated by Hfq, we have studied the structures of DsrA and DsrA/*rpoS* complex by NMR. We have shown that, in this research, DsrA contains a dynamic conformational equilibrium for its second stem–loop which might be an important mechanism for DsrA to regulate the translations of its multiple target mRNAs.

Flexible region in the SL1 pentaloop is important for *rpoS* binding

The RNA hairpin loops are frequently structured and can play an important role by acting as nucleation sites for the three-dimensional folding of the entire molecule (44). Studies on RNA pentaloops show that many of these hairpins form structures with additional, unusual hydrogen-bonding and base-pairing interactions. For example, the CUCAA terminal pentaloop of helix 21 (nucleotides 618–622) of the *E. coli* 16S rRNA forms a non-planar A-C-A triple base interaction to stabilize the loop structure (45). Another GCUAA pentaloop of the central region of the human R/G stem–loop pre-mRNA forms a sheared G–A mismatch by the first and last nucleotides of the loop (46). Therefore, we would like to learn whether A11 and C15 of DsrA-SL1 can form an A–C mismatch base pair, or if A11 and the other three uridines can form A-U Watson–Crick base pair at the stem–loop junction. However, there is no evidence for any hydrogen bonding or sequence specific interactions observed in the loop region that can contribute to the stability of the loop structure.

Previous mutagenesis studies showed that DsrA-SL1 lost its activity to activate *rpoS* translation with most of the mutations in the AUUUC pentaloop. However, the biological significances relating to these five nucleotides do not seem to be the same. The first nucleotide (A11) is not so critical, while the fifth nucleotide (C15) is highly selective (22). From the structure of DsrA-SL1 we deduced, A11 exhibits the A-form helix characteristic while C15 is free from the helix region and its structure is highly flexible. In addition, all the five loop nucleotides participate into the formation of an A-form helix in the structure of DsrA/*rpoS* complex (Figure 4A and D). These results suggest that the loop nucleotides in DsrA-SL1 may play more important roles in base-pairing with their target mRNAs and regulating their translation.

Complex structure of DsrA/*rpoS*

Structural knowledge of sRNA/mRNA interactions is important in understanding the function of sRNA and its target prediction and recognition. It has been demonstrated that DsrA-SL1 melts out to base pairing with the *rpoS* mRNA (47). Lease et al. has found that two conformations might exist for the DsrA/*rpoS* RNA complex constituted by full-length DsrA and minimal *rpoS* leader RNA (23). However, our binding assay showed there is only one single band of the DsrA32/rpoS25 complex at a ratio of 1:1, consistent with the result of the full-length DsrA and the full-length *rpoS* leader (25).

Although it has been well studied that both DsrA and *rpoS* can unwind their stem–loop structures to facilitate an efficient sRNA-mRNA annealing (23,32), there is no direct

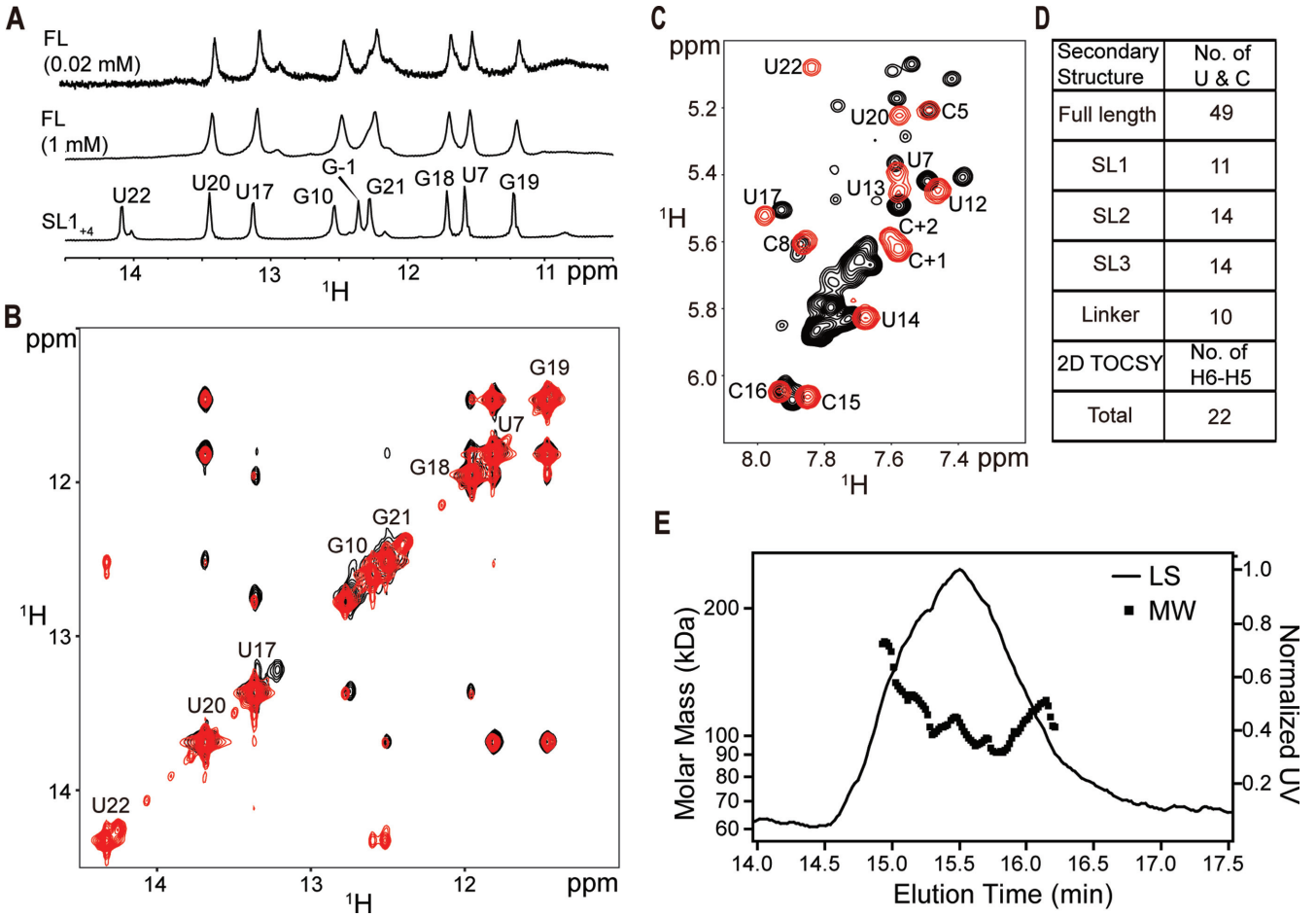

Figure 8. NMR structural studies of full-length DsrA. (**A**) Comparison of the imino regions of 1D spectra of full-length DsrA (FL) and $SL1_{+4}$. The imino proton of U22 was not observed in full-length DsrA due to rapid exchange with solvent, while it is protected by two G–C base pairs in $SL1_{+4}$. (**B**) Overlap of imino-to-imino regions of 2D ^{1}H–^{1}H NOESY of $SL1_{+4}$ (red) and full-length DsrA (1 mM, black). The resonances are labeled by the one-letter nucleotide code and the residue number. (**C**) Overlap of H6-to-H5 regions of 2D ^{1}H-^{1}H TOCSY spectrum of $SL1_{+4}$ (red) and full-length DsrA (1 mM, black). (**D**) Table of the number of uracils and cytosines in the secondary structure and number of H6-H5 cross-peaks in 2D ^{1}H–^{1}H TOCSY of full-length DsrA. (**E**) MALS measurement from SEC of 20 μM full-length DsrA at a flow rate of 0.75 ml/min. Light scattering is shown as a function of elution time (solid line, right axis). Calculated molar mass is shown for the peak (square, left axis).

structural information about the DsrA/*rpoS* complex available yet. Using NMR titration, we found that all the imino resonances belonging to DsrA-SL1 disappeared and many new signals appeared upon its binding to *rpoS* mRNA. This result is also consistent with the previous reports that the stem of DsrA-SL1 is totally unfolded and interacts with *rpoS* via base-pairing. As the NMR signals of the DsrA32/rpoS25 complex are almost the same as the R58 hairpin construct, our data indicated that the DsrA/*rpoS* complex forms a duplex structure instead of a kissing complex proposed by Lease and Belfort (21). Since there are only seven G-C Watson–Crick base pairs out of a total of 22 base pairs and several bulges in the complex, the complex structure is unstable. In addition, the nucleotides from A28 to U32 of DsrA, which are the major binding sites of Hfq, indeed base pair with *rpoS*. This is consistent with the hypothesis that Hfq cycles off the DsrA after sRNA/mRNA duplex formation (48).

Biological implication of the two conformational states of SL2

Multiple secondary structure models have been previously proposed for DsrA (Supplementary Figure S4). The only difference between these models is the fold of SL2. Although the computational analysis of DsrA sequence reveals that Domain2 has a relatively high structural flexibility (31), the reason for the existence of different secondary structures arrangements for DsrA-SL2 is largely unexplained. Interestingly, in the NMR spectra of some shortened variants of Domain2, we observed the coexistence of two different secondary structures (Fold A and B) which are consistent with those in Mode B and D, respectively. The relative populations of these two folds are changing in different variants, relying on the length of the Linker1 and the stability of the lower stem of SL2.

DsrA is a small noncoding RNA that can positively or negatively regulate the translations of multiple target mRNAs, such as *rpoS*, *hns*, *mreB* and *rbsD*. All these regulatory activities are realized by the imperfect base-pairing be-

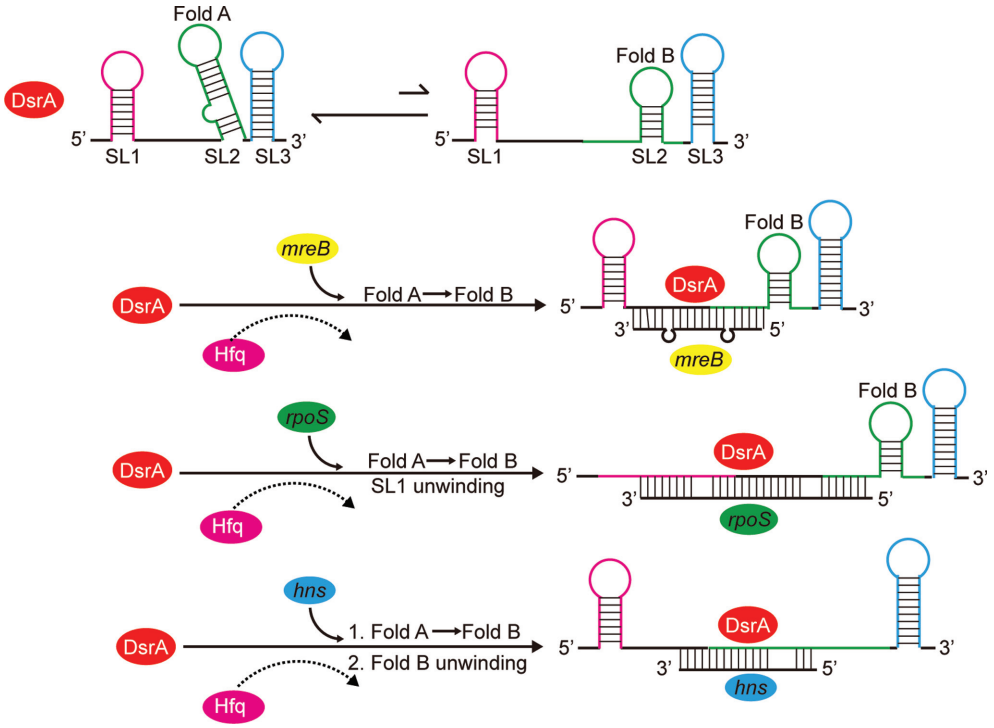

Figure 9. Model of structural selection of DsrA sRNA for adapting multiple target regulation. Three stem–loops of DsrA are colored magenta, green and blue, respectively. The single strand linkers between stem–loops are colored black. DsrA rearranges alternative conformations to adapt to different mRNAs, such as *mreB*, *rpoS* and *hns* mRNAs. The recognition of mRNAs is stimulated by binding of Hfq to free DsrA, followed by the release of Hfq from the sRNA/mRNA complex.

tween DsrA and its target mRNAs. DsrA base pairs with *rpoS* and *mreB* mRNAs using the nucleotides G10-U41 (32) and A24-U41 (42), respectively (Supplementary Figure S8). The nucleotides from U42 to U59 of SL2 that do not participate into the base-pairing with mRNA are exactly same as the sequence of Domain2$_{20nt}$ RNA, in which the Fold B is formed. The Fold B is also predicted for DsrA-SL2 in a secondary structure model proposed for the DsrA/*mreB* complex (42). In addition, the hybridization of DsrA/rpoS140 to the isoenergetic microarray also showed that DsrA-SL2 had a secondary structure of Fold B in the DsrA/*rpoS* complex (32). Together these evidences suggest that the base-pairing interaction between DsrA and certain mRNAs (*rpoS* and *mreB*) might induce a structural transition of SL2 from Fold A to Fold B, as we observed in different constructs of Domain2 RNA.

The reduced binding affinity of rpoS18 and R22 RNAs with the SL12 ΔC53 mutant (Figure 7D and F) indicates that, if DsrA forms the Model A structure with a long stem for its SL2, the three-nucleotide single-strand linker between SL1 and SL2 is insufficient for an efficient base-pairing between DsrA and mRNA. On the other hand, if DsrA forms the Model B structure with a stable Fold A for the SL2, the nucleotides 31–34 would be the only nucleotides free for the base-pairing with *hns* mRNA. We therefore speculated that the conformational plasticity of DsrA maybe an important reason to explain why DsrA can efficiently regulate the translations of multiple target mRNAs using the imperfect base-pairing.

Based on our NMR experiments, a working model is proposed to explain the role of conformational plasticity of DsrA sRNA in the regulation of multiple mRNAs translation (Figure 9). Before binding to mRNAs, DsrA has different conformations and the major population adopts the same secondary structure as Model B (Fold A). Upon base pairing with the complementary sequence in the mRNAs, such as *rpoS* and *merB* mRNA, DsrA converts its major conformation from Fold A to Fold B. In case of *hns* mRNA, because the sequence that DsrA used to base pair with *hns* contains the portion of Fold B, Fold B will have to unwind upon the interaction. This unwinding process has been confirmed by our NMR titration and other's isoenergetic microarray mapping results (32). Based on previous work, the recognition of mRNAs is stimulated by binding of Hfq to free DsrA, followed by the release of Hfq from the sRNA/mRNA complex (23). In summary, DsrA uses an interesting mechanism of conformational selection to efficiently interact with different regulatory target mRNAs, in which the conformational plasticity of DsrA-SL2 plays a crucial role.

DsrA can form oligomeric states at high concentration

It has been shown by native PAGE, there were three DsrA RNA species: monomer form, dimers and/or oligomeric forms, and polymers (35). The relative ratio of polymers increases with the increasing of the RNA concentration, up to ∼30% when the RNA concentration is only 3 μM (35). As the concentration of our NMR sample of the full-length

DsrA is more than 0.02 mM, it is likely that most DsrA in our sample forms polymers. As a matter of fact, we could only observe the signals of SL1 for the full-length DsrA in the NMR spectrum, suggesting that DsrA may has an oligomeric state in solution, which is also confirmed by our SEC-MALS experiment.

Using atomic force microscopy (AFM) and fluorescence microscopy, DsrA was observed to self-assemble into long filaments and much larger, more complex nanostructures (34). DsrA filaments are predicted to be formed with coaxial stacking of 14-bp (5′-CUUGCUUAAGCAAG-3′) and 8-bp (5′-AAGUGCUU-3′) duplexes from successive self-assembled DsrA monomers (34). To form DsrA 2D/3D nanostructures, the addition of a third duplex is expected to induce lateral interactions between individual DsrA filaments. A weakly paired 12-bp (5′-AACGAAUUUUUU-3′) duplex is predicted to be the third duplex needed (34). However, we found that not only SL2 but also SL3 unfolded at high concentration of full-length DsrA in our NMR studies. We observed that the signal of $SL3_{+4}$ RNA was as good as $SL1_{+4}$, and SL3 signals had very good linewidth and intensity in SL23 RNA. As good signals of SL1 were observed in the spectra of the full-length DsrA, we could rule out the possibility that the absence of SL2 and SL3 signals is due to the large molecular weight of DsrA polymers. These results together suggest that SL3, which could form a much stronger duplex than 12-bp, may be the third duplex to induce lateral interactions between DsrA filaments and to form extended nanostructures. Although DsrA remains the only natural RNA that can self-assemble into nanostructures at high concentrations *in vitro* (34), the further investigation of its high-order structure at low concentration *in vivo* is potentially meaningful.

COORDINATE DEPOSITION

Coordinates for the 20 lowest energy structures of DsrA-SL1 have been deposited in the Protein Data Bank under accession code 5WQ1, and chemical shifts have been deposited in the BioMagResBank under accession code 26934.

SUPPLEMENTARY DATA

Supplementary Data are available at NAR Online.

ACKNOWLEDGEMENTS

We thank Dr Michael Summers, Dr Xiao Heng, Dr Na Zhang, Dr Yang Zou, Dr Weiwei Wang and Dr Lijun Wang for helpful discussions. We thank Dr Zhijun Liu and Dr Ke Ruan for assistance with NMR data collection; Dr Zhiyong Zhang for assistance with NMR structure calculation and refinement; Dr Yunxing Wang for kindly providing the plasmid of T7 RNA polymerase; F. Delaglio and A. Bax for providing the software NMRPipe; T.D. Goddard and D. Kneller for Sparky; W.L. Delano for PyMol. Some of our NMR work was performed at the National Center for Protein Science Shanghai.

FUNDING

Ministry of Science and Technology of China [2016YFA0500700]; Strategic Priority Research Program of the Chinese Academy of Sciences [XDB08010100, XDB08030302]; Chinese National Natural Science Foundation [31330018, 31270782, 91540103]. Funding for open access charge: Ministry of Science and Technology of China [2016YFA0500700]; Strategic Priority Research Program of the Chinese Academy of Sciences [XDB08010100].
Conflict of interest statement. None declared.

REFERENCES

1. Waters,L.S. and Storz,G. (2009) Regulatory RNAs in bacteria. *Cell*, **136**, 615–628.
2. Gottesman,S. and Storz,G. (2011) Bacterial small RNA regulators: versatile roles and rapidly evolving variations. *Cold Spring Harbor Perspecti. Biol.*, **3**, a003798.
3. Storz,G., Vogel,J. and Wassarman,K.M. (2011) Regulation by small RNAs in bacteria: expanding frontiers. *Mol. Cell*, **43**, 880–891.
4. Gottesman,S. (2004) The small RNA regulators of Escherichia coli: roles and mechanisms*. *Annu. Rev. Microbiol.*, **58**, 303–328.
5. Jousselin,A., Metzinger,L. and Felden,B. (2009) On the facultative requirement of the bacterial RNA chaperone, Hfq. *Trends Microbiol.*, **17**, 399–405.
6. Nielsen,J.S., Boggild,A., Andersen,C.B., Nielsen,G., Boysen,A., Brodersen,D.E. and Valentin-Hansen,P. (2007) An Hfq-like protein in archaea: crystal structure and functional characterization of the Sm protein from Methanococcus jannaschii. *RNA*, **13**, 2213–2223.
7. Mackie,G.A., Coburn,G.A., Miao,X., Briant,D.J., Prud'homme-Genereux,A., Stickney,L.M. and Hankins,J.S. (2008) Preparation of the Escherichia coli RNase E protein and reconstitution of the RNA degradosome. *Methods Enzymol.*, **447**, 199–213.
8. Scheibe,M., Bonin,S., Hajnsdorf,E., Betat,H. and Morl,M. (2007) Hfq stimulates the activity of the CCA-adding enzyme. *BMC Mol. Biol.*, **8**, 92.
9. Wassarman,K.M. (2007) 6S RNA: a regulator of transcription. *Mol. Microbiol.*, **65**, 1425–1431.
10. Glaeser,J., Zobawa,M., Lottspeich,F. and Klug,G. (2007) Protein synthesis patterns reveal a complex regulatory response to singlet oxygen in Rhodobacter. *J. Proteome Res.*, **6**, 2460–2471.
11. Heidrich,N., Moll,I. and Brantl,S. (2007) In vitro analysis of the interaction between the small RNA SR1 and its primary target ahrC mRNA. *Nucleic Acids Res.*, **35**, 4331–4346.
12. Baker,C.S., Eory,L.A., Yakhnin,H., Mercante,J., Romeo,T. and Babitzke,P. (2007) CsrA inhibits translation initiation of Escherichia coli hfq by binding to a single site overlapping the Shine-Dalgarno sequence. *J. Bacteriol.*, **189**, 5472–5481.
13. Morita,T. and Aiba,H. (2006) RNA silencing mediated by small RNAs in Escherichia coli. *Tanpakushitsu kakusan koso. Protein Nucleic Acid Enzyme*, **51**, 2478–2483.
14. Sledjeski,D. and Gottesman,S. (1995) A small RNA acts as an antisilencer of the H-NS-silenced rcsA gene of Escherichia coli. *Proc. Natl. Acad. Sci. U.S.A.*, **92**, 2003–2007.
15. Sledjeski,D.D., Gupta,A. and Gottesman,S. (1996) The small RNA, DsrA, is essential for the low temperature expression of RpoS during exponential growth in Escherichia coli. *EMBO J.*, **15**, 3993–4000.
16. Repoila,F. and Gottesman,S. (2003) Temperature sensing by the dsrA promoter. *J. Bacteriol.*, **185**, 6609–6614.
17. Repoila,F. and Gottesman,S. (2001) Signal transduction cascade for regulation of RpoS: temperature regulation of DsrA. *J. Bacteriol.*, **183**, 4012–4023.
18. Bak,G., Han,K., Kim,D. and Lee,Y. (2014) Roles of rpoS-activating small RNAs in pathways leading to acid resistance of Escherichia coli. *Microbiol. Open*, **3**, 15–28.
19. Cayrol,B., Fortas,E., Martret,C., Cech,G., Kloska,A., Caulet,S., Barbet,M., Trepout,S., Marco,S., Taghbalout,A. *et al.* (2014) Riboregulation of the bacterial actin-homolog MreB by DsrA small noncoding RNA. *Integrative Biol.: Quant. Biosci. Nano to Macro*, **7**, 128–141.

20. Aiba,H. (2007) Mechanism of RNA silencing by Hfq-binding small RNAs. *Curr. Opin. Microbiol.*, **10**, 134–139.
21. Lease,R.A. and Belfort,M. (2000) A trans-acting RNA as a control switch in Escherichia coli: DsrA modulates function by forming alternative structures. *Proc. Natl. Acad. Sci. U.S.A.*, **97**, 9919–9924.
22. Majdalani,N., Cunning,C., Sledjeski,D., Elliott,T. and Gottesman,S. (1998) DsrA RNA regulates translation of RpoS message by an anti-antisense mechanism, independent of its action as an antisilencer of transcription. *Proc. Natl. Acad. Sci. U.S.A.*, **95**, 12462–12467.
23. Lease,R.A. and Woodson,S.A. (2004) Cycling of the Sm-like protein Hfq on the DsrA small regulatory RNA. *J. Mol. Biol.*, **344**, 1211–1223.
24. Sledjeski,D.D., Whitman,C. and Zhang,A. (2001) Hfq is necessary for regulation by the untranslated RNA DsrA. *J. Bacteriol.*, **183**, 1997–2005.
25. Soper,T.J. and Woodson,S.A. (2008) The rpoS mRNA leader recruits Hfq to facilitate annealing with DsrA sRNA. *RNA*, **14**, 1907–1917.
26. Resch,A., Vecerek,B., Palavra,K. and Blasi,U. (2010) Requirement of the CsdA DEAD-box helicase for low temperature riboregulation of rpoS mRNA. *RNA Biol.*, **7**, 796–802.
27. McCullen,C.A., Benhammou,J.N., Majdalani,N. and Gottesman,S. (2010) Mechanism of positive regulation by DsrA and RprA small noncoding RNAs: pairing increases translation and protects rpoS mRNA from degradation. *J. Bacteriol.*, **192**, 5559–5571.
28. Sedlyarova,N., Shamovsky,I., Bharati,B.K., Epshtein,V., Chen,J., Gottesman,S., Schroeder,R. and Nudler,E. (2016) sRNA-mediated control of transcription termination in E. coli. *Cell*, **167**, 111–121.
29. Lease,R.A., Cusick,M.E. and Belfort,M. (1998) Riboregulation in Escherichia coli: DsrA RNA acts by RNA:RNA interactions at multiple loci. *Proc. Natl. Acad. Sci. U.S.A.*, **95**, 12456–12461.
30. Ribeiro Ede,A. Jr, Beich-Frandsen,M., Konarev,P.V., Shang,W., Vecerek,B., Kontaxis,G., Hammerle,H., Peterlik,H., Svergun,D.I., Blasi,U. *et al.* (2012) Structural flexibility of RNA as molecular basis for Hfq chaperone function. *Nucleic Acids Res.*, **40**, 8072–8084.
31. Rolle,K., Zywicki,M., Wyszko,E., Barciszewska,M.Z. and Barciszewski,J. (2006) Evaluation of the dynamic structure of DsrA RNA from E. coli and its functional consequences. *J. Biochem.*, **139**, 431–438.
32. Fratczak,A., Kierzek,R. and Kierzek,E. (2011) Isoenergetic microarrays to study the structure and interactions of DsrA and OxyS RNAs in two- and three-component complexes. *Biochemistry*, **50**, 7647–7665.
33. Geinguenaud,F., Gesson,M. and Arluison,V. (2014) Thermodynamic aspects of the self-assembly of DsrA, a small noncoding RNA from Escherichia coli. *Acta Biochim. Polon.*, **61**, 179–184.
34. Cayrol,B., Nogues,C., Dawid,A., Sagi,I., Silberzan,P. and Isambert,H. (2009) A nanostructure made of a bacterial noncoding RNA. *J. Am. Chem. Soc.*, **131**, 17270–17276.
35. Cayrol,B., Geinguenaud,F., Lacoste,J., Busi,F., Le Derout,J., Pietrement,O., Le Cam,E., Regnier,P., Lavelle,C. and Arluison,V. (2009) Auto-assembly of E. coli DsrA small noncoding RNA: molecular characteristics and functional consequences. *RNA Biol.*, **6**, 434–445.
36. Papenfort,K. and Vogel,J. (2009) Multiple target regulation by small noncoding RNAs rewires gene expression at the post-transcriptional level. *Res. Microbiol.*, **160**, 278–287.
37. Sharma,C.M., Darfeuille,F., Plantinga,T.H. and Vogel,J. (2007) A small RNA regulates multiple ABC transporter mRNAs by targeting C/A-rich elements inside and upstream of ribosome-binding sites. *Genes Dev.*, **21**, 2804–2817.
38. Wohnert,J., Gorlach,M. and Schwalbe,H. (2003) Triple resonance experiments for the simultaneous correlation of H6/H5 and exchangeable protons of pyrimidine nucleotides in 13C,15N-labeled RNA applicable to larger RNA molecules. *J. Biomol. NMR*, **26**, 79–83.
39. Lybecker,M., Bilusic,I. and Raghavan,R. (2014) Pervasive transcription: detecting functional RNAs in bacteria. *Transcription*, **5**, e944039.
40. Durney,M.A. and D'Souza,V.M. (2010) Preformed protein-binding motifs in 7SK snRNA: structural and thermodynamic comparisons with retroviral TAR. *J. Mol. Biol.*, **404**, 555–567.
41. Majdalani,N., Vanderpool,C.K. and Gottesman,S. (2005) Bacterial small RNA regulators. *Crit. Rev. Biochem. Mol. Biol.*, **40**, 93–113.
42. Cayrol,B., Fortas,E., Martret,C., Cech,G., Kloska,A., Caulet,S., Barbet,M., Trepout,S., Marco,S., Taghbalout,A. *et al.* (2015) Riboregulation of the bacterial actin-homolog MreB by DsrA small noncoding RNA. *Integr. Biol.: Quant. Biosci. Nano to Macro*, **7**, 128–141.
43. Lalaouna,D., Morissette,A., Carrier,M.C. and Masse,E. (2015) DsrA regulatory RNA represses both hns and rbsD mRNAs through distinct mechanisms in Escherichia coli. *Mol. Microbiol.*, **98**, 357–369.
44. Uhlenbeck,O.C. (1990) Tetraloops and RNA folding. *Nature*, **346**, 613–614.
45. Nagaswamy,U., Gao,X.L., Martinis,S.A. and Fox,G.E. (2001) NMR structure of a ribosomal RNA hairpin containing a conserved CUCAA pentaloop. *Nucleic Acids Res.*, **29**, 5129–5139.
46. Stefl,R. and Allain,F.H. (2005) A novel RNA pentaloop fold involved in targeting ADAR2. *RNA*, **11**, 592–597.
47. Lease,R.A. and Belfort,M. (2000) Riboregulation by DsrA RNA: trans-actions for global economy. *Mol. Microbiol.*, **38**, 667–672.
48. Peng,Y., Curtis,J.E., Fang,X. and Woodson,S.A. (2014) Structural model of an mRNA in complex with the bacterial chaperone Hfq. *Proc. Natl. Acad. Sci. U.S.A.*, **111**, 17134–17139.